Dynamic volume-rendered optical coherence tomography pupillometry

Peter M Maloca[1,2,3,4*], Emanuel R de Carvalho[4], Pascal W Hasler[2-3], Konstantinos Balaskas[4,7], Nadja Inglin[1], Axel Petzold[4-6], Catherine Egan[4], Adnan Tufail[4], Hendrik P N Scholl[1-3], Philippe Valmaggia[1]

[1]Institute of Molecular and Clinical Ophthalmology Basel (IOB), Basel, Switzerland
[2]OCTlab, Department of Ophthalmology, University Hospital Basel, Basel, Switzerland
[3]Department of Ophthalmology, University of Basel, Basel, Switzerland
[4]Moorfields Eye Hospital, London, UK
[5]National Hospital for Neurology and Neurosurgery, UCLH & UCL Institute of Neurology, Queen Square, London, UK
[6]Dutch Expertise Centre Neuro-ophthalmology, Amsterdam UMC, NL
[7]Moorfields Ophthalmic Reading Centre, London, UK

Abstract word count: 250 / 250; Total word count: 4001

*Corresponding author: Peter Maloca, Institute of Molecular and Clinical Ophthalmology Basel (IOB), Basel, Switzerland, Telephone +41 61 265 87 87, Fax Fax +41 61 265 87 43, E-mail: peter.maloca@iob.ch, ORCID iD 0000-0002-4794-5859

Conflicts of interest: Adnan Tufail received a portion of funding from the Department of Health's NIHR Biomedical Research Centre for Ophthalmology at Moorfields Eye Hospital and UCL Institute of Ophthalmology, United Kingdom, and is a consultant for Heidelberg Engineering. Peter Maloca owns intellectual properties on speckle denoising. Peter Maloca and Pascal Hasler receive lecture fees from Heidelberg. Dr. Scholl is member of the Scientific Advisory Board of: Astellas Institute for Regenerative Medicine; Gensight Biologics; Ionis Pharmaceuticals, Inc.; Gyroscope Therapeutics Ltd.; Janssen Research & Development, LLC (Johnson & Johnson); and Pharma Research & Early Development (pRED) of F. Hoffmann-La Roche Ltd; Novartis Pharma AG (CORE). Dr. Scholl is paid consultant of: Boehringer Ingelheim Pharma GmbH & Co; Gerson Lehrman Group; and Guidepoint. Dr. Scholl is member of the Data Monitoring and Safety Board/Committee of Belite Bio and ReNeuron Group Plc/Ora Inc. and member of the Steering Committee of Novo Nordisk (FOCUS trial). Dr. Scholl is co-director of the Institute of Molecular and Clinical Ophthalmology Basel (IOB) which is constituted as a non-profit foundation and receives funding from the University of Basel, the University Hospital Basel, Novartis, and the government of Basel-Stadt. These arrangements have been reviewed and approved by the University of Basel (Universitätsspital Basel, USB) in accordance with its conflict of interest policies.
Dr. Scholl is principal investigator of grants at the USB sponsored by the following entities: IVERIC bio (Ophthotech Corporation); Kinarus AG; and Novartis Pharma AG. Grants at USB are negotiated and administered by the institution (USB) which receives them on its proper accounts. Individual investigators who participate in the sponsored project(s) are not directly compensated by the sponsor but may receive support from the institution for their project(s). Others: none.

Abstract

Purpose: To assess intrapupillary space (IPS) changes in healthy subjects with regard to decreased iris motility in patients with pseudoexfoliation glaucoma (PEXG) or nonarteritic anterior ischaemic optic neuropathy (NAION) in a clinical environment.

Methods: Scotopic and photopic IPS measurements using three-dimensionally rendered swept-source optical coherence tomography (SS-OCT) data were obtained and compared for all subjects. IPS parameters were evaluated such as absolute volumetric differences, relative light response for volumetric ratios and pupillary ejection fraction (PEF) for functional contraction measurements.

Results: From a total of 122 IPS from 66 subjects, 106 IPS were eligible for comparison providing values for 72 normal, 30 PEXG and 4 NAION eyes. In healthy, PEXG and NAION subjects, scotopic overall mean IPS was 8.90, 3.45 and 4.16 mm^3, and photopic overall mean IPS was 0.87, 0.74 and 1.13 mm^3, respectively. Three-dimensional contractility showed a mean absolute difference of 8.03 mm^3 for mormals (defined as 100% contractility), 2.72 mm^3 for PEXG (33.88% of normal) and 3.03 mm^3 for NAION (38.50% of normal) with a relative light response ratio between scotopic and photopic volumes of 10.26 (100%), 4.69 (45.70%) and 3.67 (35.78%), respectively. PEF showed a contractile pupillary emptying of 88.11% for normals, 76.92% for PEXG and 70.91% for NAION patients.

Conclusion: This 3D pupillometry OCT (pOCT) assessment allows for quantitative measurements of pupil function, contractility and response to light. More specifically, PEF is presented as a potential (neuro)-pupillary outcome measure that could be useful in the monitoring of ophthalmic disorders that affect pupillary function.

Keywords: pupillary ejection fraction, contractility, optical coherence tomography, pseudoexfoliation glaucoma, nonarteritic anterior ischaemic optic neuropathy

Introduction

The aqueous humor, produced at a rate of 2-3 µl/min in an epithelial bilayer covering the ciliary body (Brubaker 1991), traverses the posterior iris surface and the anterior lens surface to reach the anterior chamber via the pupil. It is then cleared by the outflow apparatus of the trabecular meshwork (Mark 2010). The size and shape of the pupil is influenced by the intensity and color of the incident light and regulated by the dilator and the sphincter muscle, which are mainly innervated by the sympathetic and parasympathetic branches of the autonomic nervous system (McDougal & Gamlin 2015).

The pupillary reaction has been studied as the pupillary light reflex (PLR) which denotes the immediate narrowing of the pupil with brief illumination, followed by a rapid widening when the light stimulus ends (Kelbsch et al. 2019). The PLR is usually estimated subjectively, without proper quantification while others set the PLR standards so high that it will be very demanding to bring them into clinical practice. Its velocity and amplitude have been difficult to quantify. A variety of factors can impair the normal function of the pupil and alter the PLR. The intrinsic neuromuscular pathway of the iris muscle can be compromised with pathology of the sympatic and parasympatic system which includes dysautonomia in diseases such as diabetes mellitus (Park et al. 2017; Ba-Ali et al. 2020), optic neuropathies (Munch et al. 2015), and neurodegenerative conditions such as Alzheimer's disease (Kremen et al. 2019) or Parkinson's disease (Joyce et al. 2018). Typically, in anterior ischemic optic neuropathy (AION) an incomplete pupil response due to ischemic damage of the optic nerve head perfusion is found (Tsika et al. 2015). A pathologic PLR has also been found in glaucoma (Kankipati et al. 2011; Tekin et al. 2019), retinitis

pigmentosa (Kardon et al. 2011; Kawasaki et al. 2012), and age-related macular degeneration (AMD) (Maynard et al. 2015). In pseudoexfoliation (PEX) syndrome, pupil malfunction occurs due to the accumulation of fibrillogranular material causing infiltration and fibrosis of the iris and other parts in the body in (Scharfenberg et al. 2019). If an imbalance between AH production and AH outflow is observed, elevated intraocular eye pressure can lead to pseudoexfoliative glaucoma (PEXG) which if left untreated can result in blindness (Denis et al. 1994).

Although PLR can easily be generated by a flashlight, quantitative results allow a more objective assessment of the pupil circuitry. Currently, most PLR devices use a two-dimensional infrared imaging approach to record pupil diameter changes under changing light conditions (Atchison et al. 2011; Smith et al. 2019). Ideally, such measurements would be performed in a clinical environment and not require laboratory-controlled conditions (Kelbsch et al. 2019) or specially trained operators.

In recent years, optical coherence tomography (OCT) has become a routine clinical imaging tool for anterior eye segment measurements, e.g. of the iris and the pupil, among other structures (Huang et al. 1991; Aptel & Denis 2010; Koktekir et al. 2014; Fujimoto & Huang 2016; Schuster et al. 2017). The structural-functional relationship between the pupil light reflex and macular ganglion cells is relevant for the clinical differential diagnosis (Meneguette et al. 2019).

In this study, we regard the pupil as a “watergate”, given its function as an important barrier between the posterior and anterior chambers of the eye (Dvoriashyna et al. 2018). At the same time, we expand the scope of current two-dimensional anterior segment OCT imaging by assessing a dynamic volumetric pupillometry OCT (pOCT)

method that provides a novel three-dimensional analysis of pupillary function in healthy and diseased eyes.

Materials and Methods

Ethics statement and subjects

All procedures involving human participants were in accordance with the ethical standards of the institutional and/or national research committee and with the 1964 Helsinki declaration and its later amendments or comparable ethical standards. Written informed consent was obtained from all subjects, and the study was cleared by the Ethics Committee Zentral und Ostschweiz, Switzerland (EKNZ TIBE-15/90).
In this first 3D OCT pupillometry study, we collected randomly data from healthy subjects and patients visiting the clinic and known to be associated with a disorder of pupillary motility. Thus, each subject contributed one eye or pupil volume per side. Patients were requested for study participation in the order of their arrival at the clinic, so that the number of patients probably corresponds to a usual frequency of the corresponding disease within an outpatient eye clinic.
The inclusion criteria for the healthy control group were age above 18 years and the absence of any ocular disease. The inclusion criteria for the PEXG patients were visualization of white PEX deposit on the pupil margin and on the anterior lens surface using conventional slit-lamp examination and the need for topical treatment for elevated intraocular pressure. In the NAION group, patients who had a history of clinically proven and laboratory verified NAION were included. The healthy eye in the NAION group was not included for analysis. Exclusion criteria for all groups were history of ocular surgery, ocular trauma, abnormalities of the pupil, a positive history of neurodegenerative diseases, such as Alzheimer or Parkinson disease or the use of drugs with possible impairment of pupil function.

Swept-source optical coherence tomography of the pupil

In summary, one eye was measured per subject and categorized into the three classes (normal, PEXG and AION). For reproducibility of the method, one volume was labeled by several graders and the obtained values were verified for repeatability.

In detail, the recording of the OCT volumes was carried out as follows: A commercially available swept-source OCT (SS-OCT) device was used (OCT DRI OCT-1 Atlantis, software version 9.12.003.04, Topcon, Tokyo, Japan). An advantage of the OCT system was, that the scanning beam is centered at a wavelength of 1050 nm and is therefore invisible to the human eye and therefore not affecting the pupils. A convex lens, preinstalled by the manufacturer, was placed and the scan focus was set on the corneal epithelium to provide the auto-adjustment for an image with maximum signal intensity. The manufacturer's built-in and smallest internal fixation target (one single square) was used in all subjects to reduce the perceived luminance so that the pupil size was not altered by the target during the experiment wherever possible. Patients were instructed to adopt a position as relaxed as possible to prevent possible accommodation.

Data recording

The SS-OCT measurement was triggered as soon as the pupil was centered in the middle of the recording display and the iris-lens diaphragm was positioned as orthogonal as possible to the direction of the laser beam. Image acquisition per eye consisted of 256 cross-sectional images per volume of the pupil-lens diaphragma with a standard scan pattern over a 6.0 mm x 6.0 mm x 2.6 mm area centered on the anterior lens apex with a scan density of 512 x 128 pixels (Fig. 1).

The first measurement in relative darkness (scotopic SS-pOCT) was performed in a darkened room and with the use of an opaque drape (Oculus, Wetzlar, Germany) to allow the pupil to dilate as much as possible and to prevent for unwanted light leakage. The second measurement (photopic SS-pOCT) was performed by simulating sunlight using an adjustable daylight therapy lamp that provides a flicker-free and UV-free light (Beurer TL 90, Ulm, Germany) depicted in Fig. 1. According to the manufacturer, this medical device emits with a light intensity of approximately 10,000 lux in a distance of 15 cm with a color temperature of 6500 Kelvin. Keeping the recommended safety distance, the lamp was positioned to the side of the subject's head in a 90 degrees angle and switched on in the examination room with common room brightness. The fellow eye was not covered separately. However, care was taken to ensure that the fellow eye was not directly illuminated. The scan data was saved and exported as a sequence of 256 bmp images (512 x 992 pixels each) directly from the scanner for further image processing.

Fundus photographs were not acquired, in order to avoid unnecessary exposure of the eye to light. No eye drops with effects on pupil function were used.

Data processing and image analysis

The OCT images were freed from speckle-noise to enhance the visibility of the anterior lens and iris surface and binary data were produced (Fig. 2) (C. Gyger 2014). These images were imported into the software ImageJ (Version 1.48b) to delineate a three-dimensional intrapupillary space (IPS). Horizontal and vertical borders were marked at the corresponding pupillary edge in the vertical and horizontal axis using the en face image display of the built-in crop (3D) viewer (Schindelin 2012). The exterior border was defined using the center B-scan of the image stack and a linear plan was manually set using the software's ruler tool at an

off-set of 200 pixels above the anterior lens surface. Finally, the inner border of the IPS was defined by the reflective structure of the anterior lens surface provided by the OCT image.

The resulting IPS images were imported to Amira Software® 5.6.0 (Thermo Fisher Scientific, Waltham, USA) to render a three-dimensional IPS model allowing for calculations of its volume and surface area based on a triangular surface grid created for an object embedded in a voxel dataset. The same procedure was applied for all eyes.

Pupillary ejection fraction

The pupil as a volume contains the aqueous humor which proceeds from the posterior to the anterior chamber. To evaluate the percentage of aqueous humor "pumped" out during a pupillary contraction, the following formula was used:

$$Pupillary\ Ejection\ Fraction\ [\%] = \frac{Scotopic\ Volume\ [mm^3] - Photopic\ Volume\ [mm^3]}{Scotopic\ Volume\ [mm^3]} x\ 100$$

This PEF calculation is analogous to the calculation of the left ventricular ejection fraction of the heart representing the central measure of left ventricular systolic function (Kosaraju & Makaryus 2020). The cutoff level was defined as the mean value of the normal group.

3D Contractility

The measurement of the IPS in three dimensions allows to quantify the aqueous humor leaving the pupil. To measure the absolute volumetric difference between the scotopic and photopic volumes, and hereby evaluate how much aqueous humor the pupil pumps out with a contraction, we calculate the 3D contractility as following:

$$3D\ Contractility\ [mm^3] = Scotopic\ Volume\ [mm^3] - \ Photopic\ Volume\ [mm^3]$$

Relative light response

The ratio between the different volumes was calculated and denoted relative light response. This relative light response represents the ratio between the scotopic and the photopic volume. By this formula, we show how much more aqueous humor is inside the pupil in mydriasis compared to miosis:

$$Relative\ light\ response\ [Ratio] = \frac{Scotopic\ Volume\ [mm^3]}{Photopic\ Volume\ [mm^3]}$$

In order to compare the different subgroups (normal, PEXG or NAION) with each formula, the mean values were calculated for each sub-group first. The mean values of the normal versus the patient group were then set as a relative benchmark of 100% and compared to the mean values of the comparison groups PEXG and NAION. Therefore, we present the PEF as a functional value of the pupil, the 3D contractility as the absolute change and the relative light response as the ratio between the photopic and scotopic measurements.

Furthermore, these formulas were used to calculate the differences of surface areas measured in mm^2 of the scotopic and photopic pupils.

Statistical analysis

The statistical analysis was carried out with RStudio (Team 2014) v3.6.0 (R Foundation for Statistical Computing, Vienna, Austria). Q-Q plots were used to assess normal distribution of the data. ANOVA tests were used to identify differences between all groups. Wilcoxon rank sum tests were used to compare

groups with non-normal distributed data, student's t-test were used in case of normal distribution. Paired t-tests were used for comparisons between scotopic and photopic data points within the groups.

The data is presented as mean ± standard deviation. The calculations for statistical significance were performed for a p-value of <0.05. Grades of significance were labelled as following in the figures and tables: not significant (n.s.) ≙ $p \geq 0.05$, * ≙ $0.05 > p \geq 0.01$, ** ≙ $0.01 > p \geq 0.001$, *** ≙ $0.001 > p \geq 0.0001$, **** ≙ $0.0001 > p$. The graphs were also produced with R 3.6.0 using RStudio.

Reproducibility of the IPS measurements

To test the reproducibility of the IPS measurement method, one pupil was manually segmented three times by three independent graders. Reproducibility was assessed by determining the mean, the standard deviation, and the Coefficient of Variation (CoV) for the volume and surface area measurements, for each of the three graders and for the measurements of the three graders combined. CoV measures the ratio of the standard deviation to the mean (Everitt 1998) and indicates the amount of variability relative to the mean of the population. Intra-grader and inter-grader variability were analyzed for volume and surface area measurement separately by one-way Analysis of Variance (ANOVA). This is the decomposition of the total sum of squares (SS_{tot}) into grader sum of squares (SS_{grader}) and residual sum of squares ($SS_{residual}$). SS_{grader} and $SS_{residual}$ indicate how much of the total variability is attributable to inter-grader and intra-grader variability, respectively. F-tests were performed to investigate the effect of different graders on the measurements.

Results

Patient characteristics

A total of 66 subjects of Caucasian origin were included in this study and completed volume scans in 122 eyes. Each included eye was measured with a wide and narrow pupil contributing 244 volumes in total. The cohort consisted of 40 female and 26 male participants. Their mean age was 65.1 years and their refractive error ranged from +4 to -7.25 spherical diopters. 40 normal subjects contributed 160 volumes and were assigned to the normal group. 18 subjects suffered from PEXG and contributed 68 volumes. 8 patients suffered from NAION and contributed 16 volumes.

From a total of 122 eyes, 106 were eligible after excluding 16 measurements because of image artifacts (8 normals, 4 PEXG and 4 NAION due to pseudophakia, respectively). Thus, 72 normals, 30 PEXG and 4 NAION eyes were included for the final analysis. The IPS measurements are summarized in Table 1 and Table 2. Representative images from IPS renderings are depicted in Fig. 3.

Normal distribution

In order to evaluate the normal distribution, QQ-Plots were generated for the scotopic and photopic volumes and surface areas and for the absolute differences between them. The normal and PEXG data were assessed as normally distributed. The NAION data was spread out and hence not normally distributed which is probably due to the low sample number. As the QQ-plots are similar for scotopic and photopic volumes within the different groups, QQ-plots of the absolute volumetric differences are shown in Fig. 4.

Non-parametric ANOVA tests (Kruskal-Wallis tests) were performed to compare the three groups as the NAION data was not normally distributed. The tests were statistically significant for all calculated endpoints ($p < 0.0001$). For a pairwise

comparison between the groups Wilcoxon rank sum tests were used to compare NAION to normal and PEXG data, student's t-test were used to compare normal and PEXG data.

Volume evaluations

Within the different groups all differences between mydriasis and miosis were statistically significant. In the normal group the mean PEF was 88.12 ± 6.96 %, the mean 3D contractility was 8.03 ± 4.72 mm^3 ($p < 0.0001$) and the mean relative light response was 10.26 ± 4.15. In the PEXG group, the mean PEF was 76.92 ± 11.49 %, mean 3D contractility was 2.72 ± 1.15 mm^3 ($p < 0.0001$), the mean relative light response was 4.69 ± 1.80. In the NAION group the mean PEF was 70.91 ± 29.47 %, mean 3D contractility was 3.03 ± 1.39 mm^3 ($p = 0.0225$), the mean relative light response was 3.67 ± 2.95.

Statistically significant differences were found between the normal and remaining disease groups. Statistical significance was not reached for comparison of the two disease groups. When comparing the PEXG group to the normal group, the PEXG eyes indicated a smaller PEF (87.29%, $p < 0.0001$), lower 3D contractility (33.88%, $p < 0.0001$) and a lower relative light response (45.69%, $p < 0.0001$). The NAION eyes showed a smaller PEF for NAION (80.47%, $p = 0.0161$), a lower 3D contractility (38.50%, $p = 0.0206$) and a lower relative light response (41.75%, $p = 0.0161$). The comparison between PEXG and NAION pupils showed neither statistically significant differences in the mean PEF ($p = 0.3365$), mean 3D contractility ($p = 0.5529$), and mean relative light response ($p = 0.3365$). The results of the volumetric comparisons with PEF, 3D contractility and relative light response are displayed in Fig. 5.

Surface area measurements

Besides the evaluations of the volumes, the contractility and the relative light response were evaluated for the surface area measurements. A PEF evaluation for the surface area was omitted, as the PEF is specifically intended to represent the fraction of a volume.

Similar to the volumetric analyses, all differences between scotopic and photopic measurements were statistically significant within the different groups. In the normal group the mean contractility for the surface area was 32.62 ± 16.22 mm^2 ($p < 0.0001$), the mean surface area ratio was 6.05 ± 2.04. In the PEXG group the mean absolute difference was 12.85 ± 5.00 mm^2 ($p < 0.0001$), the mean surface area ratio was 3.49 ± 1.07. In the NAION group the mean contractility was 12.56 ± 6.37 mm^2 ($p = 0.0291$), the mean surface area ratio was 2.524 ± 1.60.

The surface area comparisons between the groups showed statistically significant differences between the disease groups with the normal group and no statistically significant difference for the comparison between PEXG and NAION. The comparison of the PEXG and the normal group showed a smaller mean contractility (39.40%, $p < 0.0001$) and relative light response (57.66% $p < 0.0001$) for the PEXG group. A normal with NAION comparison indicated a smaller absolute (38.50%, $p = 0.0095$) and relative (41.75%, $p = 0.0083$) surface area change. The comparison between PEXG and NAION pupils showed neither in the mean contractility ($p = 0.9384$) nor in the mean relative light response ($p = 0.8569$) statistically significant results.

Reproducibility of the method

The F-test statistic indicated that no grader measured significantly differently from the other graders with p-values of 0.496 and 0.350 for the volume and surface area measurements, respectively. The described method showed a very high reproducibility indicated by the small Coefficient of Variation (CoV) values ranging from 0.0058 to 0.0217. This holds within individual graders as well as when the measurements of the three graders are combined. Inter-grader variability accounts for 20.8% (29.5%) and intra-grader variability for 79.2% (70.5%) of the total variability for volume (surface area) as measured by the decomposition of the total sum of squares (SS_{tot}) into the grader sum of squares (SS_{grader}) and the residual sum of squares ($SS_{residual}$). The results are summarized in Table 3.

Discussion

Dynamics of the aqueous humor have reasonably been modelled based on living and cadaver eyes (Abouali et al. 2012; Villamarin et al. 2012; Modarreszadeh et al. 2014; Wang et al. 2016). In our method, the pupil is regarded as a “watergate”, a deformable physical cavity that redirects different volumes of aqueous humor. We propose a novel quantitative and dynamic volumetric pupillometry OCT (pOCT) method to assess pupil function, applied in a clinical environment and under real-life conditions. Thus, a widely used and commercially available OCT device with an added external light source was successfully developed and employed in healthy subjects and PEXG and NAION patients. The proposed pOCT proved to be a feasible and reproducible technique, capable of enhancing previous pupillometry methods with novel spatial information.

Using an approach similar to the one used in the calculation of the cardiac ejection fraction, quantitative measurements of the PEF were ascertained, providing a tissue and structure-based assessment of the pupillary geometry and functionality as a valve (Miller 2018). Under scotopic conditions, both the volume and surface area of the IPS was higher in all groups when compared to photopic conditions, as ascertained with a newly described 3D contractility parameter. The relative light response, which can be regarded as a volumetric marker, demonstrated a decreased pupillary response to at least half or more in eyes affected by PEXG or NAION compared to the healthy control group.

Decline in pupillary dilation in PEXG has been previously reported (Watson et al. 1995; Jonas et al. 2013; You et al. 2013; Fernandez-Vigo et al. 2018) and our results fall within the range reported in these studies, albeit on the lower end (Suzuki & Kurimoto 1992; Yulek et al. 2008; Ulviye Y 2015). The methodology and parameters applied in these studies, namely the use of basic diameter pupil diameters, differs from our method. On the other hand, our method relied on more sustained light exposure and of higher intensity which might have led to a more pronounced pupillary reaction.

Eyes with PEXG showed significant reduced amplitude of pupil contraction values compared to healthy eyes (Tekin et al. 2018; Tekin et al. 2019). This could be helpful in the evaluation of spatial conditions prior to cataract surgery and aid in the estimation of the success rate of drug or surgical pupil extension interventions at an early stage (Akman et al. 2004; Fontana et al. 2017; Grzybowski & Kanclerz 2020).

The pupillary light response, constriction ratio, velocity and latency are decreased both in the acute and chronic phases of NAION, and our results corroborate the findings of other studies (Herbst et al. 2013; Tsika et al. 2015; Yoo et al. 2017).

The differences in pupillary motility between PEXG and NAION are driven by distinct pathophysiological mechanisms. The pupillary constriction latency may reflect delay in afferent visual processing in NAION, while mechanical in PEXG (Vazquez & Lee 2014; Miller & Arnold 2015). In this study, a similar range of quantitative pupil motility values were found in both disorders, with no specific differences. In addition, atrophy of the ganglion cell layer in NAION and other optic neuropathies affecting only one eye is strongly correlated with quantitative assessment of the pupil light reflex (Meneguette et al. 2019).

Amongst the limitations of our study, we identified the following: The OCT device was not developed for pupil measurements of the anterior segment but for posterior segment analysis. The current OCT acquisition time of 2.9 seconds per volume measurement was relatively long and only monocular recordings without tracking technology could be acquired. A comparison with spectral-domain OCT devices was not yet performed with regard to the proposed method. Compared to SD-OCT, SS-OCT has particular advantages as uses a wave length centred around 1050 nm and provides a scan beam outside the optically detectable range for the eye, so that the iatrogenic light effect on pupil function is negligible. This also prevents a subject from following the scan beam instead of focusing on the fixation target, which would inevitably lead to measurement errors. Thus, the properties of SS-OCT, i.e. no pupil interference and high data acquisition to avoid motion artifacts, render it more suitable for pupil function measurements. With more advanced OCT devices, which measure at a sampling frequency around 1.6 GHz, a pupil measurement at intervals

of up to 0.18 seconds would theoretically be possible, so that the spatial and temporal resolution could be massively improved (Xu et al. 2015; Maertz et al. 2018; Siddiqui et al. 2018; Porporato et al. 2020).

In contrast to a flashlight test, the current method is too laborious. However, such a flashlight test is usually performed with different light sources, completely different angles and distances to the eye. Therefore, the incident light intensity is very variable leading to a poor reproducibility. In contrast, our proposed method is a measurement based on structural data with defined spacing, showed good reproducibility and is relatively objective. Therefore, the values would also be quite homogeneous between different investigators and centers, which represents a clinical benefit. We understand that this will be assessed in further studies. We envision that in the future such a method can be automatically delivered with new OCT generations and this will contribute to more objective data and enhance clinical practice. Especially in the case of small defects of pupillary motility, for example in the early stage of optic neuritis, the defect may be very small and not detectable by an ordinary flashlight test, which may lead to diagnostic uncertainty and time delay. On the other hand, such small abnormalities could well be detected by a structural pOCT method. Another limitation was that in the current configuration, swinging-flashlight exposure was not used. The light source was not adaptable in light intensity, color and size. This led to a full-field light stress in the examined eye and precluded stimulation of specific pupil sectors. The spatial range was limited as solely measurements with maximum and minimum light intensity were used. Consequently to this, it was not possible to provide enhanced dynamic videos or extensive comparisons regarding minute differences of the pupil response, including latency or speed (Winston et al. 2020).

Nevertheless, the used light source was suitable for generating data, easy to use and affordable. Acquisition was conducted in adults only, precluding assessment of age-specific normative values. No automatic image processing was applied, but this could be addressed in upcoming studies. As a current limit of the study it must be mentioned that a correlation between visual field defects and the extent of pupillary function impairment was not the subject of this study, but this may be possible in the future with further studies. Interference from room illumination was not considered but kept stable during the entire study. Likewise, it was not possible to measure in absolute darkness because a fixation object had to be presented to guide the patient. The smallest object in terms of area was used to minimize unwanted exposure to light. Patients with NAION reported that the fixation target was relatively difficult to focus on causing a slightly unsteady fixation. The method required phakic eyes, as the anterior surface of the lens was used as a delineating border. The alignment of the pupil within the field of view and its positioning perpendicular to the laser beam was one of the main challenges. OCT provides limited visibility posterior to the iris pigment epithelium. Therefore, if there is an excess of iris tissue, fluid-filled space just below the pupillary border cannot be measured reliably (Schuster et al. 2017). In addition, the IPS was cropped in a square, meaning individual pupil shapes cannot be taken into account. The choice of offset for the outer segmentation line was arbitrary. The AMIRA version used did not allow direct measurements of the surface areas and hence approximative calculations (CoV 2.7%) had to be used. The axial lengths of the bulbi were not measured or compared in this study and thus not considered. Age and gender were not considered in this feasibility study and differences could be investigated in follow-up studies. Although the AION group was very interesting, due to the short time period in this first feasibility study, it was not

possible to collect enough AION patients to offer sufficient data for a rigorous statistical analysis. Thus, the number of subjects was relatively small, especially in the NAION group (n=4) and statistical analyses including this group are to be interpreted with this restraint. Nevertheless, the few cases of euphakic NAION patients showed distinctive deviations, so that these values were nevertheless included in this manuscript as an example but will have to be further investigated later in studies with a representative number of subjects.

Despite all these limitations, the method proved to be applicable under daily clinical conditions, using a commercial and widely available OCT device, and without the need to set up expensive and complex laboratory settings to assess the pupil function.

Conclusions

This feasibility study showed that pOCT allows quantitative measurement of pupil dynamics in healthy and diseased eyes based on structural information. Its scope could potentially be expanded in the assessment of multiple ophthalmic disorders that affect pupil function, and the PEF could potentially be used as a novel (neuro)-pupillary outcome measure obtained under clinical conditions.

Data Availability Statement

All data relevant to the study are included in the article.

References

Abouali O, A Modareszadeh, A Ghaffarieh & J Tu (2012): Investigation of saccadic eye movement effects on the fluid dynamic in the anterior chamber. Journal of biomechanical engineering **134**: 021002.

Akman A, G Yilmaz, S Oto & YA Akova (2004): Comparison of various pupil dilatation methods for phacoemulsification in eyes with a small pupil secondary to pseudoexfoliation. Ophthalmology **111**: 1693-1698.

Aptel F & P Denis (2010): Optical coherence tomography quantitative analysis of iris volume changes after pharmacologic mydriasis. Ophthalmology **117**: 3-10.

Atchison DA, CC Girgenti, GM Campbell, JP Dodds, TM Byrnes & AJ Zele (2011): Influence of field size on pupil diameter under photopic and mesopic light levels. Clinical & experimental optometry **94**: 545-548.

Ba-Ali S, AE Brondsted, HU Andersen, P Jennum & H Lund-Andersen (2020): Pupillary light responses in type 1 and type 2 diabetics with and without retinopathy. Acta ophthalmologica.

Brubaker RF (1991): Flow of aqueous humor in humans [The Friedenwald Lecture]. Investigative ophthalmology & visual science **32**: 3145-3166.

C. Gyger CC, R; Hasler, PW; Maloca, P (2014): Three-dimensional speckle reduction in optical coherence tomography through structural guided filtering. Opt. Eng. **53**: 73105.

Denis P, JP Nordmann, PP Elena, H Saraux & P Lapalus (1994): Central nervous system control of intraocular pressure. Fundamental & clinical pharmacology **8**: 230-237.

Dvoriashyna M, R Repetto, MR Romano & JH Tweedy (2018): Aqueous humour flow in the posterior chamber of the eye and its modifications due to pupillary block and iridotomy. Mathematical medicine and biology : a journal of the IMA **35**: 447-467.

Everitt BS (1998): The cambridge dictionary of statistics cambridge university press. Cambridge, UK Google Scholar

Fernandez-Vigo JI, L de-Pablo Gomez de Liano, I Sanchez-Guillen, A Macarro-Merino, C Fernandez-Vigo, J Garcia-Feijoo & JA Fernandez-Vigo (2018): Pseudoexfoliation signs in the anterior segment assessed by optical coherence tomography and Scheimpflug device. Archivos de la Sociedad Espanola de Oftalmologia **93**: 53-59.

Fontana L, M Coassin, A Iovieno, A Moramarco & L Cimino (2017): Cataract surgery in patients with pseudoex-foliation syndrome: current updates. Clinical ophthalmology (Auckland, N.Z.) **11**: 1377-1383.

Fujimoto J & D Huang (2016): Foreword: 25 Years of Optical Coherence Tomography. Investigative ophthalmology & visual science **57**: OCTi-OCTii.

Grzybowski A & P Kanclerz (2020): Methods for achieving adequate pupil size in cataract surgery. Current opinion in ophthalmology **31**: 33-42.

Herbst K, B Sander, H Lund-Andersen, M Wegener, J Hannibal & D Milea (2013): Unilateral anterior ischemic optic neuropathy: chromatic pupillometry in affected, fellow non-affected and healthy control eyes. Frontiers in neurology **4**: 52.

Huang D, EA Swanson, CP Lin, JS Schuman, WG Stinson, W Chang, MR Hee, T Flotte, K Gregory, CA Puliafito & et al. (1991): Optical coherence tomography. Science **254**: 1178-1181.

Jonas JB, V Nangia, A Matin, K Bhojwani, A Sinha, A Khare, S Agarwal & K Bhate (2013): Pseudoexfoliation: normative data and associations. The Central India Eye and Medical Study. PLoS One **8**: e76770.

Joyce DS, B Feigl, G Kerr, L Roeder & AJ Zele (2018): Melanopsin-mediated pupil function is impaired in Parkinson's disease. Scientific reports **8**: 7796.

Kankipati L, CA Girkin & PD Gamlin (2011): The post-illumination pupil response is reduced in glaucoma patients. Investigative ophthalmology & visual science **52**: 2287-2292.

Kardon R, SC Anderson, TG Damarjian, EM Grace, E Stone & A Kawasaki (2011): Chromatic pupillometry in patients with retinitis pigmentosa. Ophthalmology **118**: 376-381.

Kawasaki A, SV Crippa, R Kardon, L Leon & C Hamel (2012): Characterization of pupil responses to blue and red light stimuli in autosomal dominant retinitis pigmentosa due to NR2E3 mutation. Investigative ophthalmology & visual science **53**: 5562-5569.

Kelbsch C, T Strasser, Y Chen, B Feigl, PD Gamlin, R Kardon, T Peters, KA Roecklein, SR Steinhauer, E Szabadi, AJ Zele, H Wilhelm & BJ Wilhelm (2019): Standards in Pupillography. Frontiers in neurology **10**: 129.

Koktekir BE, S Gonul, B Bakbak, S Gedik & OK Dogan (2014): The effect of room illumination on the measurement of anterior segment parameters. Eye & contact lens **40**: 181-184.

Kosaraju A & AN Makaryus (2020): Left Ventricular Ejection Fraction StatPearls. Treasure Island (FL).

Kremen WS, MS Panizzon, JA Elman, EL Granholm, OA Andreassen, AM Dale, NA Gillespie, DE Gustavson, MW Logue, MJ Lyons, MC Neale, CA Reynolds, N Whitsel & CE Franz (2019): Pupillary dilation responses as a midlife indicator of risk for Alzheimer's disease: association with Alzheimer's disease polygenic risk. Neurobiology of aging **83**: 114-121.

Maertz J, JP Kolb, T Klein, KJ Mohler, M Eibl, W Wieser, R Huber, S Priglinger & A Wolf (2018): Combined in-depth, 3D, en face imaging of the optic disc, optic disc pits and optic disc pit maculopathy using swept-source megahertz OCT at 1050 nm. Graefe's archive for clinical and experimental ophthalmology = Albrecht von Graefes Archiv fur klinische und experimentelle Ophthalmologie **256**: 289-298.

Mark HH (2010): Aqueous humor dynamics in historical perspective. Survey of ophthalmology **55**: 89-100.

Maynard ML, AJ Zele & B Feigl (2015): Melanopsin-Mediated Post-Illumination Pupil Response in Early Age-Related Macular Degeneration. Investigative ophthalmology & visual science **56**: 6906-6913.

McDougal DH & PD Gamlin (2015): Autonomic control of the eye. Comprehensive Physiology **5**: 439-473.

Meneguette NS, JER de Carvalho & A Petzold (2019): A 30 s test for quantitative assessment of a relative afferent pupillary defect (RAPD): the infrared pupillary asymmetry (IPA). Journal of neurology **266**: 969-974.

Miller LW (2018): Cardiac Ejection Fraction: New Insights About its Dynamic Nature. Journal of the American College of Cardiology **72**: 602-604.

Miller NR & AC Arnold (2015): Current concepts in the diagnosis, pathogenesis and management of nonarteritic anterior ischaemic optic neuropathy. Eye (Lond) **29**: 65-79.

Modarreszadeh S, O Abouali, A Ghaffarieh & G Ahmadi (2014): Physiology of aqueous humor dynamic in the anterior chamber due to rapid eye movement. Physiology & behavior **135**: 112-118.

Munch M, L Leon, S Collomb & A Kawasaki (2015): Comparison of acute non-visual bright light responses in patients with optic nerve disease, glaucoma and healthy controls. Scientific reports **5**: 15185.

Park JC, YF Chen, NP Blair, FY Chau, JI Lim, YI Leiderman, M Shahidi & JJ McAnany (2017): Pupillary responses in non-proliferative diabetic retinopathy. Scientific reports **7**: 44987.

Porporato N, M Baskaran, R Husain & T Aung (2020): Recent advances in anterior chamber angle imaging. Eye (London, England) **34**: 51-59.

Scharfenberg E, FG Rauscher, P Meier & D Hasenclever (2019): Pseudoexfoliation syndrome: analysis of systemic comorbidities of 325 PEX-positive patients compared with 911 PEX-negative patients. Graefe's archive for clinical and experimental ophthalmology = Albrecht von Graefes Archiv fur klinische und experimentelle Ophthalmologie **257**: 2471-2480.

Schindelin JA-CIF, E. et al. (2012): NIH Image to ImageJ: 25 years of image analysis. Nature methods **9**: 671-675.

Schuster AK, JE Fischer & U Vossmerbaeumer (2017): Curvature of iris profile in spectral domain optical coherence tomography and dependency to refraction, age and pupil size - the MIPH Eye&Health Study. Acta ophthalmologica **95**: 175-181.

Siddiqui M, AS Nam, S Tozburun, N Lippok, C Blatter & BJ Vakoc (2018): High-speed optical coherence tomography by circular interferometric ranging. Nature photonics **12**: 111-116.

Smith J, O Flower, A Tracey & P Johnson (2019): A comparison of manual pupil examination versus an automated pupillometer in a specialised neurosciences intensive care unit. Australian critical care : official journal of the Confederation of Australian Critical Care Nurses.

Suzuki R & S Kurimoto (1992): Intraocular muscle function in pseudoexfoliation syndrome. Ophthalmologica. Journal international d'ophtalmologie. International journal of ophthalmology. Zeitschrift fur Augenheilkunde **204**: 192-198.

Tekin K, H Kiziltoprak, MA Sekeroglu, E Yetkin, S Bayraktar & P Yilmazbas (2019): Static and dynamic pupil characteristics in pseudoexfoliation syndrome and glaucoma. Clinical & experimental optometry.

Tekin K, MA Sekeroglu, H Kiziltoprak, E Yetkin, S Doguizi & P Yilmazbas (2018): Static and Dynamic Pupillary Characteristics in Clinically Unilateral Pseudoexfoliation Syndrome. Journal of glaucoma **27**: 552-557.

Tsika C, SV Crippa & A Kawasaki (2015): Differential monocular vs. binocular pupil responses from melanopsin-based photoreception in patients with anterior ischemic optic neuropathy. Scientific reports **5**: 10780.

Ulviye Y OI, Tufan AK, et al. (2015): Assessment of Pupil Diameters in Pseudoexfoliation Syndrome under Scotopic, Mesopic, Photopic and Dynamic Conditions Using Infrared Pupillometer (Assessment of Pupil Diameters in Pseudoexfoliation Syndrome). British Journal of Medicine and Medical Research **7**: 877-883.

Vazquez LE & RK Lee (2014): Genomic and proteomic pathophysiology of pseudoexfoliation glaucoma. Int Ophthalmol Clin **54**: 1-13.

Villamarin A, S Roy, R Hasballa, O Vardoulis, P Reymond & N Stergiopulos (2012): 3D simulation of the aqueous flow in the human eye. Medical engineering & physics **34**: 1462-1470.

Wang W, X Qian, H Song, M Zhang & Z Liu (2016): Fluid and structure coupling analysis of the interaction between aqueous humor and iris. Biomedical engineering online **15**: 133.

Watson NJ, S Winder & FD Green (1995): Pupil dilatation in the pseudoexfoliation syndrome. Eye (London, England) **9 (Pt 3)**: 341-343.

Winston M, A Zhou, CM Rand, EC Dunne, JJ Warner, LJ Volpe, BA Pigneri, D Simon, T Bielawiec, SC Gordon, SF Vitez, A Charnay, S Joza, K Kelly, C Panicker, S Rizvydeen, G Niewijk, C Coleman, BJ Scher, DW Reed, SM Hockney, G Buniao, T Stewart, L Trojanowski, C Brogadir, M Price, AS Kenny, A Bradley, NJ Volpe & DE Weese-Mayer

(2020): Pupillometry measures of autonomic nervous system regulation with advancing age in a healthy pediatric cohort. Clinical autonomic research : official journal of the Clinical Autonomic Research Society **30**: 43-51.

Xu J, X Wei, L Yu, C Zhang, J Xu, KK Wong & KK Tsia (2015): High-performance multi-megahertz optical coherence tomography based on amplified optical time-stretch. Biomedical optics express **6**: 1340-1350.

Yoo YJ, JM Hwang & HK Yang (2017): Differences in pupillary light reflex between optic neuritis and ischemic optic neuropathy. PLoS One **12**: e0186741.

You QS, L Xu, YX Wang, H Yang, K Ma, JJ Li, L Zhang & JB Jonas (2013): Pseudoexfoliation: normative data and associations: the Beijing eye study 2011. Ophthalmology **120**: 1551-1558.

Yulek F, OO Konukseven, HB Cakmak, N Orhan, S Simsek & A Kutluhan (2008): Comparison of the pupillometry during videonystagmography in asymmetric pseudoexfoliation patients. Current eye research **33**: 263-267.

Figure legends

Fig. 1. Representation of swept-source monocular OCT pupillometry. (A) The subject looks at a fixation target inside the OCT scanner (triangle; view from above). The OCT scan beam (black arrow) is focused perpendicular to the iris-lens diaphragm (ILD). The picture illustrates the second photopic measurement with a light source (arrow head), which was positioned at right angles to the ILD (B, view from the side).

Fig. 2. Image processing in 3D-OCT pupillometry. (A) Data from the OCT device were exported as a sequence of original images. The cornea (double arrow heads) is displayed inverted because the current device was not designed for the proposed application. Nevertheless, the lens apex (single arrowhead) and the anterior eye chamber (highlighted in blue), particularly the intrapupillary space (IPS, arrow) are identifiable. (B) Horizontal and vertical borders of the proposed IPS were demarcated and cropped corresponding to the vertical and horizontal pupil edges using the en face image display. (C) 3D rendering of the anterior segment to display the effect of speckle-denoising. In the original data, the pupil border (arrow) is occluded by speckle-noise. (D) Same data as in (C) but freed from speckle-noise with a much better visualized pupil edge (arrow). Note for both renderings identical pixel intensities were applied. (E) Residual speckle noise (arrow) inside the IPS (marked in red) was removed manually. (F) This resulted in a better visualization of the lens apex (arrowhead). A proposed IPS (marked in red) was assessed and defined perpendicular to the lens apex at an axial off-set of 200 pixels (double arrow) so that the IPS was outlined in 2D. (G) All corresponding two-dimensional IPS segmentations were finally rendered into a 3D model of the proposed IPS (marked in red) to measuring its volume and surface area (inferior view of the 3D IPS model).

Fig. 3. Three-dimensional OCT (3D-OCT) anterior eye segment rendering. (A) Photopic 3D-OCT of a healthy eye in 36-year old male. En face 3D view depicts the pupillary and ciliary layer of the iris with its pigment ruff (arrowhead) at the pupillary edge, circular contraction furrows (double arrowhead), protruding iris collarettes (arrow) and Fuchs' crypts (double arrow). (B) Posterior view of the same eye depicting the iris-lens diaphragm shows the radial contraction furrows (arrowhead), part of the lens (arrow) and the structural folds of Schwalbe (double arrow). (C) 3D model rendering of the same eye as in (A, B) shows photopic (arrowhead) and scotopic intrapupillary space (arrow) to illustrate effect of pupillary contraction. (D) Rendering of PEX material located on the anterior lens which was shovelled by the iris movement to the center of the pupil (arrowhead). (E) Close-up from (D) showing multiple elevated PEX filaments (arrow) at the pupillary edge that eventually can be flushed away by the aqueous humor to clog the anterior chamber angle and cause high intraocular eye pressure. (F) 3D rendering in a NAION patient who had more difficulties with fixation, which led to movement artifacts (arrows) resulting in a slightly deformed pupil border (arrowhead).

Fig. 4. Quantile-quantile plots for volumetric differences of the different patient groups. The plots compare the sample quantiles to the theoretical quantiles and indicate normal distribution for the normal group (n=72) (A) and the PEXG (n=30) (B) group, and a non-normal distribution for the NAION (n=4) (C) group.

Fig. 5. Comparison of pupillary ejection fraction (PEF) (A), 3D contractility (B) and the relative light responsive ratio (C) between the different patient groups and normals (n=72), PEXG (n=30) and NAION (n=4). The figures indicate a difference in the light response between the healthy and normals and both the PEXG and the

NAION group regarding PEF, 3D contractility and the light response ratio. No statistically significant difference has been found between the PEXG and the NAION group.

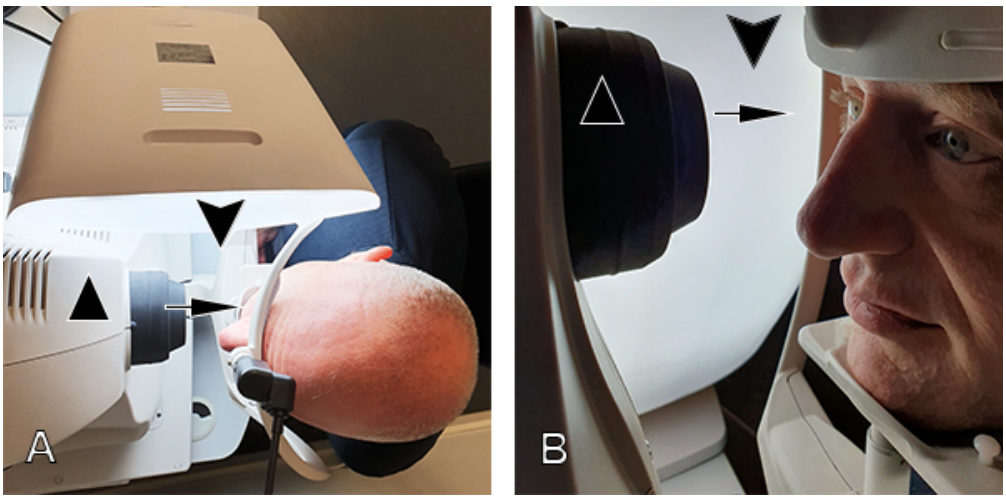

Fig. 1. Representation of swept-source monocular OCT pupillometry. (A) The subject looks at a fixation target inside the OCT scanner (triangle; view from above). The OCT scan beam (black arrow) is focused perpendicular to the iris-lens diaphragm (ILD). The picture illustrates the second photopic measurement with a light source (arrow head), which was positioned at right angles to the ILD (B, view from the side).

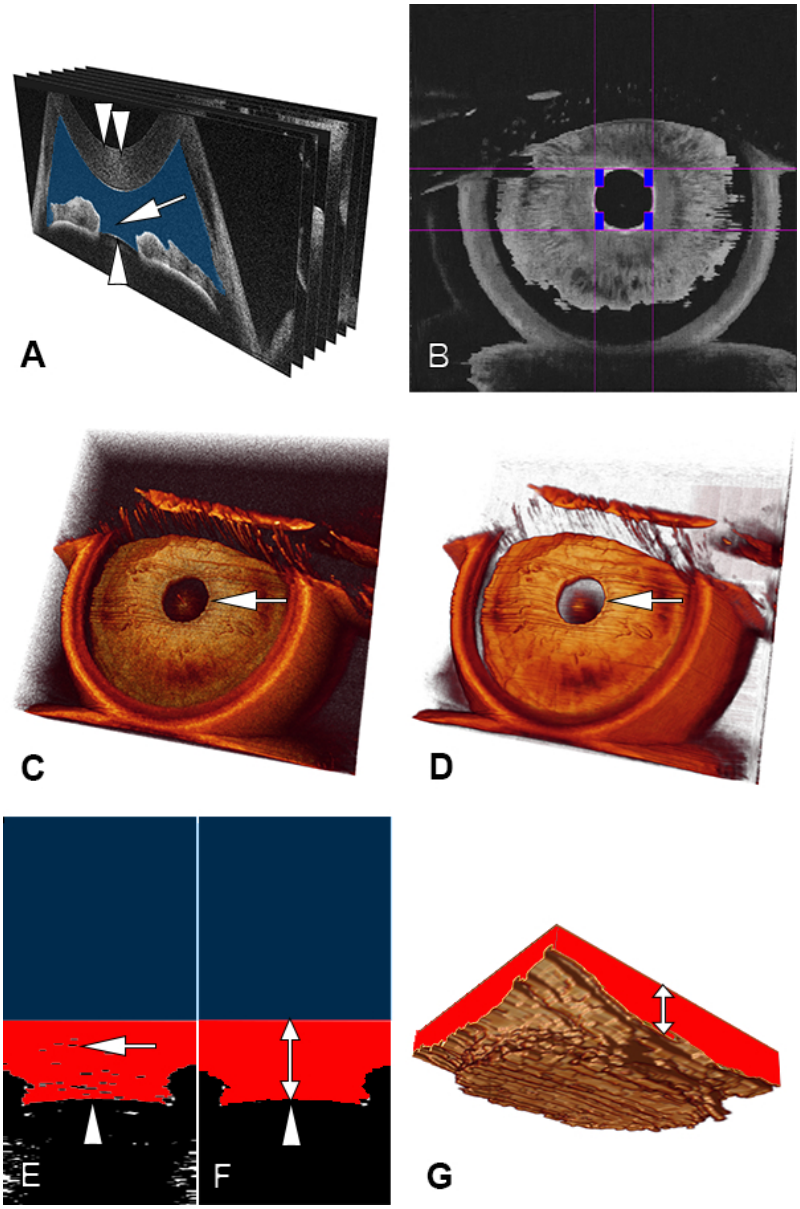

Fig. 2. Image processing in 3D-OCT pupillometry. (A) Data from the OCT device were exported as a sequence of original images. The cornea (double arrow heads) is displayed inverted because the current device was not designed for the proposed application. Nevertheless, the lens apex (single arrowhead) and the anterior eye chamber (highlighted in blue), particularly the intrapupillary space (IPS, arrow) are identifiable. (B) Horizontal and vertical borders of the proposed IPS were demarcated and cropped corresponding to the vertical and horizontal pupil edges using the en face image display. (C) 3D rendering of the anterior segment to display the effect of speckle-denoising. In the original data, the pupil border (arrow) is occluded by speckle-noise. (D) Same data as in (C) but freed from speckle-noise with a much better visualized pupil edge (arrow). Note for both renderings identical pixel intensities were applied. (E) Residual speckle noise (arrow) inside the IPS (marked in red) was removed manually. (F) This resulted in a better visualization of the lens apex (arrowhead). A proposed IPS (marked in red) was assessed and defined perpendicular to the lens apex at an axial off-set of 200 pixels (double arrow) so that the IPS was outlined in 2D. (G) All corresponding two-dimensional IPS segmentations were finally rendered into a 3D model of the proposed IPS (marked in red) to measuring its volume and surface area (inferior view of the 3D IPS model).

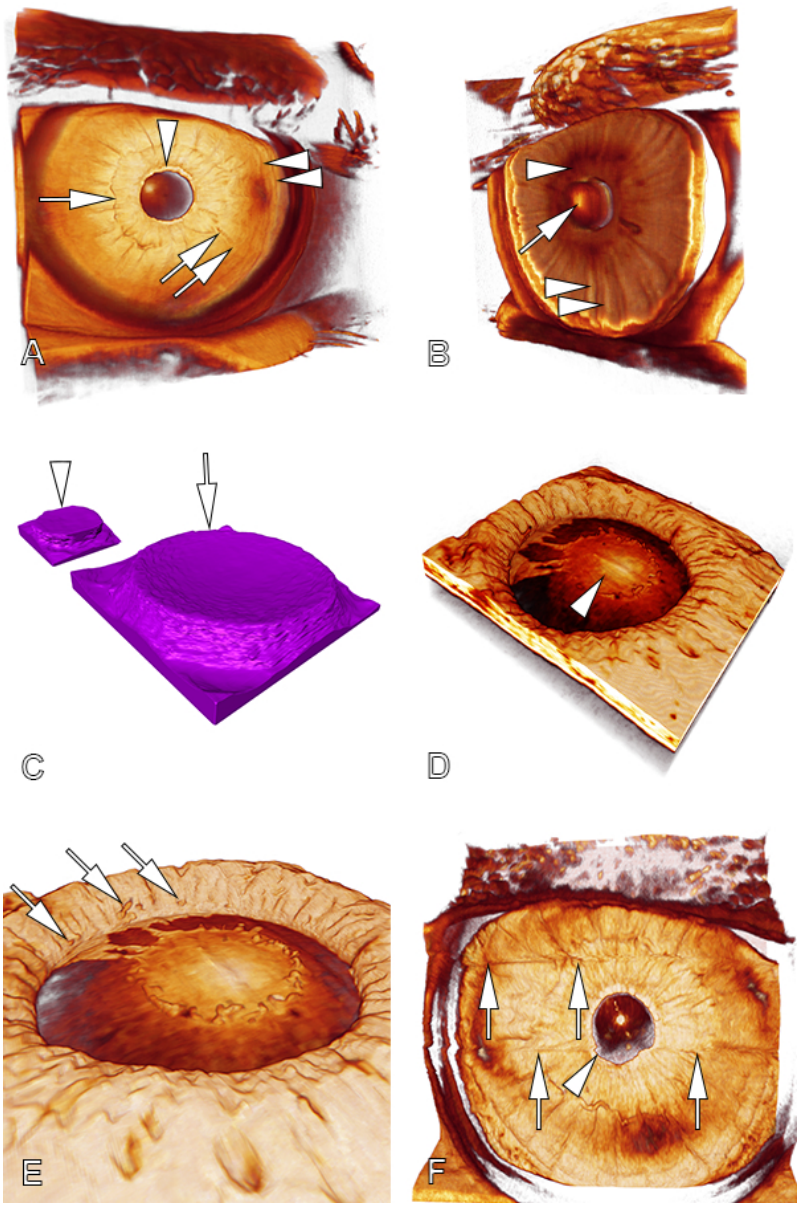

Fig. 3. Three-dimensional OCT (3D-OCT) anterior eye segment rendering. (A) Photopic 3D-OCT of a healthy eye in 36-year old male. En face 3D view depicts the pupillary and ciliary layer of the iris with its pigment ruff (arrow head) at the pupillary edge, circular contraction furrows (double arrow head), protruding iris collarettes (arrow) and Fuchs' crypts (double arrow). (B) Posterior view of the same eye depicting the iris-lens diaphragm shows the radial contraction furrows (arrow head), part of the lens (arrow) and the structural folds of Schwalbe (double arrow). (C) 3D model rendering of the same eye as in (A, B) shows photopic (arrow head) and scotopic intrapupillary space (arrow) to illustrate effect of pupillary contraction. (D) Rendering of PEX material located on the anterior lens which was shovelled by the iris movement to the center of the pupil (arrow head). (E) Close-up from (D) showing multiple elevated PEX filaments (arrow) at the pupillary edge that eventually can be flushed away by the aqueous humor to clog the anterior chamber angle and cause high intraocular eye pressure. (F) 3D rendering in a NAION patient who had more difficulties with fixation, which led to movement artifacts (arrows) resulting in a slightly deformed pupil border (arrow head).

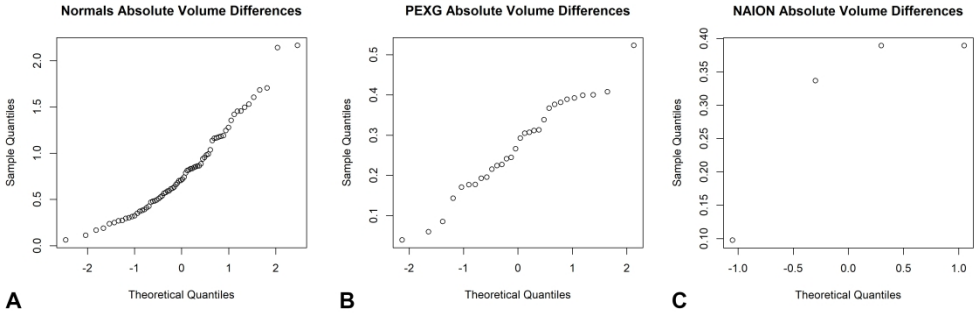

Fig. 4. Quantile-quantile plots for volumetric differences of the different patient groups. The plots compare the sample quantiles to the theoretical quantiles and indicate normal distribution for the normal group (n=72) (A) and the PEXG (n=30) (B) group, and a non-normal distribution for the NAION (n=4) (C) group.

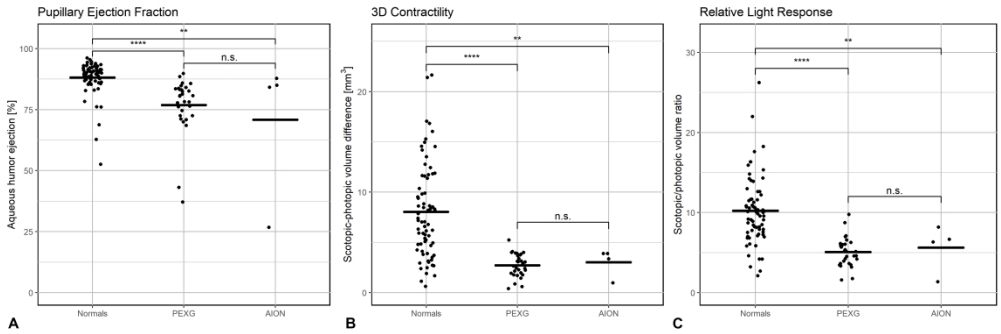

Caption : Fig. 5. Comparison of pupillary ejection fraction (PEF) (A), 3D contractility (B) and the relative light responsive ratio (C) between the different groups: normal group (n=72), PEXG (n=30) and NAION (n=4). The figures indicate a difference in the light response between the normal group and both the PEXG and the NAION group regarding PEF, 3D contractility and the light response ratio. No statistically significant difference has been found between the PEXG and the NAION group.

381x127mm (300 x 300 DPI)

Table 1. Intrapupillary space volumes in the current cohort consisting of three different groups.

	normals	PEXG	NAION
	n.s.		
		n.s.	
	n.s.		
Photopic volumes (mm^3)			
Mean	0,867	0,738	1,135
Min	0,29	0,275	0,543
Max	1,96	1,55	2,667
Standard Deviaton	0,348	0,335	1,025
	****		
		n.s.	
	*		
Scotopic volumes (mm^3)			
Mean	8,899	3,459	4,167
Min	1,158	0,873	3,641
Max	22,96	6,352	4,628
Standard Deviation	4,956	1,325	0,448
Δ Photopic – Scotopic	****	****	*

normals = healthy control group, PEXG = subjects suffering from pseudoexfoliation glaucoma (PEXG), NAION = nonarteritic anterior ischaemic optic neuropathy patient group, volume measured in in mm^3, CTRL (n=72), PEX (n=30) and NAION (n=4).

Table 2. Intrapupillary space surface area in the current cohort consisting of three different groups.

	normals	PEXG	NAION
	**		
		n.s.	
	n.s.		
Photopic surface area (mm^2)			
Mean	6,465	5,169	8,241
Min	2,74	2,827	4,334
Max	12,326	8,696	18,284
Standard Deviation	2,27	1,737	6,729
	****		
		n.s.	
	*		
Scotopic surface area (mm^2)			
Mean	39,083	18,02	20,8
Min	6,746	5,561	17,886
Max	84,346	26,883	21,902
Standard Deviation	17,663	5,909	1,947
Δ Photopic – Scotopic	****	****	*

normals = healthy control group, PEXG = subjects suffering from pseudoexfoliation glaucoma (PEXG), NAION = nonarteritic anterior ischaemic optic neuropathy patient group, surface area measured in in mm^2, CTRL (n=72), PEX (n=30) and NAION (n=4).

Table 3. Results of reproducibility measurements of three independent graders. Obtained intrapupillary space data derived from volume and surface area measurements were compared. Coefficient of Variation is given for intragrader analysis. ANOVA SSgrader represents the inter-grader variability and SSres the intra-grader variability.

Measurement	Grader	Mean (mm^3)	Std Dev (mm^3)	CoV (%)
volume	1	0,4897	0,0028	0,5806
volume	2	0,4870	0,0039	0,7998
volume	3	0,4865	0,0032	0,6585
volume	total	0,4877	0,0033	0,6671
		Mean (mm^2)	**Std Dev (mm^2)**	**CoV (%)**
surface area	1	3,8661	0,0834	2,1722
surface area	2	3,8077	0,0228	0,5966
surface area	3	3,8043	0,0333	0,8736
surface area	total	3,8260	0,0554	1,4499

ANOVA	Category	SS	SS relative	F value	P (>F)
volume (mm^3)	grader	0.000018	20.8%	0.79	0.496
volume (mm^3)	residual	0.000067	79.2%	-	-
surface area (mm^2)	grader	0.072711	29.5%	1.26	0.350
surface area (mm^2)	residual	0.173475	70.5%	-	-

Std Dev = standard deviation, CoV = coefficient of Variation, SS = sum of squares, volume measured in in mm^3, surface area measured in in mm^2.